eprints@whiterose.ac.uk
https://eprints.whiterose.ac.uk/

A Pickering Emulsion-Derived Liquid-Solid Hybrid Catalyst for Bridging Homogeneous and Heterogeneous Catalysis

Xiaoming Zhang,[†,§] Yiting Hou,[†,§] Rammile Ettelaie,[#] Ruqun Guan,[†] Ming Zhang,[†] Yabin Zhang[†] and Hengquan Yang*,[†]

[†] School of Chemistry and Chemical Engineering, Shanxi University, Taiyuan 030006, China
[#] Food Colloids Group, School of Food Science and Nutrition, University of Leeds, Leeds LS2 9JT, U.K.
Supporting Information

ABSTRACT: We describe a novel method to prepare a liquid-solid hybrid catalyst via interfacial growth of a porous silica crust around Pickering emulsion droplets, which allowed us to overcome the current limitations of both homogeneous and heterogeneous catalysts. The inner micron-scaled liquid (for example, ionic liquids) pool of the resultant catalyst can host free homogeneous molecular catalysts or enzymes to create a true homogeneous catalysis environment. The porous silica crust of the hybrid catalyst has excellent stability, which makes it amenable to packing directly in fixed-bed reactors for continuous flow catalysis. As a proof of concept, the enzymatic kinetic resolution of racemic alcohols, Cr[III](salen) complex-catalyzed asymmetric ring opening of epoxides and Pd-catalyzed Tsuji-Trost allylic substitution reactions were used to verify the generality and versatility of our strategy for bridging homogeneous and heterogeneous catalysis. The hybrid catalyst-based continuous flow system exhibited a 1.6~16-fold enhancement in activity relative to homogeneous counterparts even at more than 1500 h, and the afforded enantioselectivities were completely equal to those obtained in the homogeneous counterpart systems. Interestingly, the catalytic efficiency can be tuned through rational engineering of the porous crust and the dimensions of the liquid pool, resulting in features of an innovatively designed catalyst. This contribution provides a new method to design efficient catalysts that can bridge the conceptual and technical gaps between homogeneous and heterogeneous catalysis.

1. INTRODUCTION

The discovery of efficient catalysts is of paramount importance since most chemical reactions in industry involve catalysis. Combining the merits of both homogeneous and heterogeneous catalysts is considered an important goal for the design of powerful catalysts.[1–5] An ideal catalyst should feature well-defined active sites, high activity and exquisite selectivity like homogeneous catalysts, and insoluble solid characteristics that can be used in industrially favorable continuous flow reactors, like conventional heterogeneous catalysts.[6–8] Such a catalyst is expected to bridge the conceptual and technical gaps between homogenous and heterogeneous catalysis.[2]

Motivated by this goal, researchers have proposed many important concepts such as single site catalysts, single atom catalysts and immobilized molecular catalysts.[9–18] Although significant advances in the design of catalysts and fascinating catalytic results have been achieved, these concepts still face key challenges. For example, the immobilized molecular catalysts that are prepared by anchoring or encapsulating molecular

catalysts on or in solid supports, may be closest to realizing this goal because of the structural integration of homogeneous and heterogeneous catalysts.[19–25] Unfortunately, immobilized molecular catalysts often suffer from decreased or unpredictable activity and selectivity because of alternation of the preferred structures, the steric hindrance arising from the support surfaces or the disturbance of homogeneous microenvironments.[21,26–28] Another milestone in this direction is the supported liquid phase catalyst in which a layer of liquid that dissolves homogeneous catalysts is adsorbed onto porous solid materials.[29–32] This method, however, requires the liquid layer to be very thin and is unable to provide an ideal homogeneous microenvironment. Although encapsulated liquid catalysts have also been prepared with a surfactant-stabilized emulsion method or simple sol-gel process, these methods often lead to cracked shells or no regular morphology due to the inherent drawbacks of this emulsion with low stability or uncontrollable silica gel formation.[33–35] Recently, our group developed a method for continuous flow catalysis reactions by confining

homogeneous catalysts within Pickering emulsion droplets.[36,37] Nevertheless, this system has a limited working window since high substrate concentrations, high temperatures or high pressures lead to droplet coalescence, which fails to satisfactorily achieve the combined advantages of typical heterogeneous and homogeneous catalysis.

The above limitations urge us to seek a more ideal system in which the "microenvironment" of homogeneous catalysis, namely, "free" catalysts along with the reaction medium, are trapped within a crack-free but permeable inorganic capsule through a reliable method. Herein, we detail an unprecedented method to prepare solid-liquid hybrid catalysts based on a solid particle-stabilized emulsion (Pickering emulsion). This surfactant-free method allows us to obtain a high-quality solid-liquid hybrid catalyst that is suitable for continuous flow chemical and enzymatic reactions. The proposed catalyst particle, as shown in Figure 1A,

consists of a molecular catalyst (or enzyme)-containing ionic liquid (IL) pool and a porous solid outer crust. These types of catalyst particles are dozens of micrometers in size and are amenable to being packed in industrially preferred fixed-bed reactors for continuous flow reactions, which is analogous to conventional solid catalysts. During the reaction, reactants pass through the porous crust and encounter the molecular catalysts (or enzymes) hosted inside the IL pool, where "homogeneous" reactions occur. As exemplified by the enzymatic kinetic resolution of alcohols, Cr^{III}(salen)-catalyzed asymmetric ring opening of epoxides and Pd-catalyzed Tsuji-Trost reactions, our expectations of the superior performance of this system not only were fulfilled successfully but also were surpassed. Interestingly, the catalytic efficiency can be modulated by rationally engineering liquid-solid hybrid catalysts, which is not possible for typical homogeneous or heterogeneous catalysts.
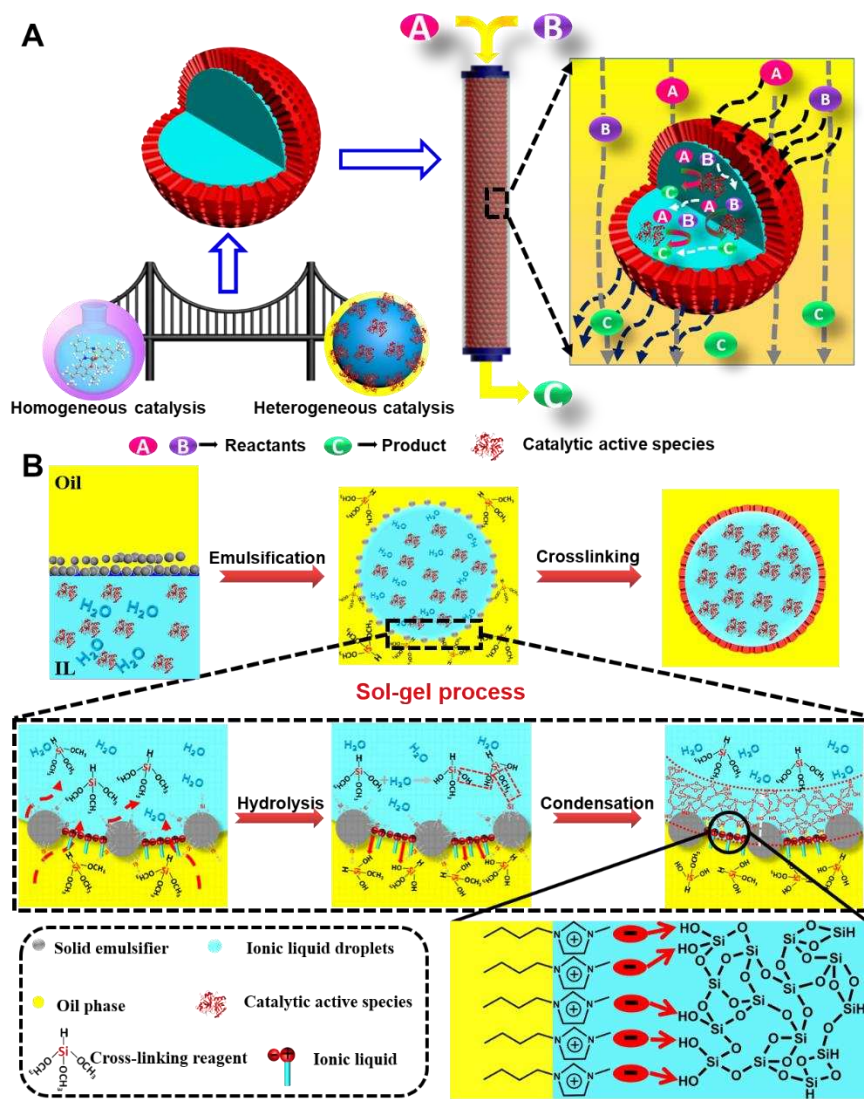

Figure 1. Construction of liquid-solid hybrid catalysts for bridging homogeneous and heterogeneous catalysis. (A) Illustration of the concept of a liquid-solid hybrid catalyst and its utilization in continuous flow reactions. (B) Schematic of the preparation procedure of a liquid-solid hybrid catalyst.

2. RESULTS AND DISCUSSION

2.1. Fabrication and Characterization of the Liquid-Solid Hybrid Capsule.

We first demonstrate the preparation of the liquid-solid hybrid capsules. We chose ILs as the inner liquid, considering their readily tailored structure and properties that enable dissolution of a wide range of homogeneous catalysts, enzymes and organic reactants.[38,39] For example, [BMIM]PF$_6$ (1-butyl-3-methylimidazolium hexafluorophosphate) [mixed with a small amount of [BMIM]BF$_4$ (1-butyl-3-methylimidazolium tetrafluoroborate) and water for growing the crust] was used as the IL phase. Solid nanoparticles were chosen as emulsifiers to stabilize the IL droplets in octane (the oil phase) because of the higher stability of Pickering emulsions and more easily tunable droplet sizes compared with surfactant-stabilized emulsions.[40–43] After screening, hydrophobic silica nanoparticles that were 20 nm in size were found to be good emulsifiers for this IL-oil mixture. [The emulsifier was prepared by modifying commercial silica

particles with dimethyldichlorosilane. Transmission electron microscopy (TEM) images, N$_2$ sorption isotherms and thermogravimetric analysis (TG) are provided in Figure S1 in the Supporting Information (SI). The methyl loading was 0.85 mmol g^{-1}. The air-water contact angle of the particle surfaces was 130°, as shown in Figure S2] As Figure 1B illustrates, the preparation process consists of two steps: 1) emulsification to obtain an IL-in-oil Pickering emulsion and 2) an interfacial sol-gel process for growing a porous crust around the IL droplets. Trimethoxysilane (TMS) or tetramethoxysilane (TMOS) was utilized as the silica precursor because they were found to be easily hydrolyzed under mild conditions and are able to form a perfect crust.

Scanning electron microscopy (SEM) images reveal that the prepared solid-liquid hybrid material comprises discrete microspheres that are 28±12 μm with smooth, crack-free surfaces (Figures 2a and b). The empty structure (after the inner liquid was removed) is visible in the SEM image of the deliberately crushed sample
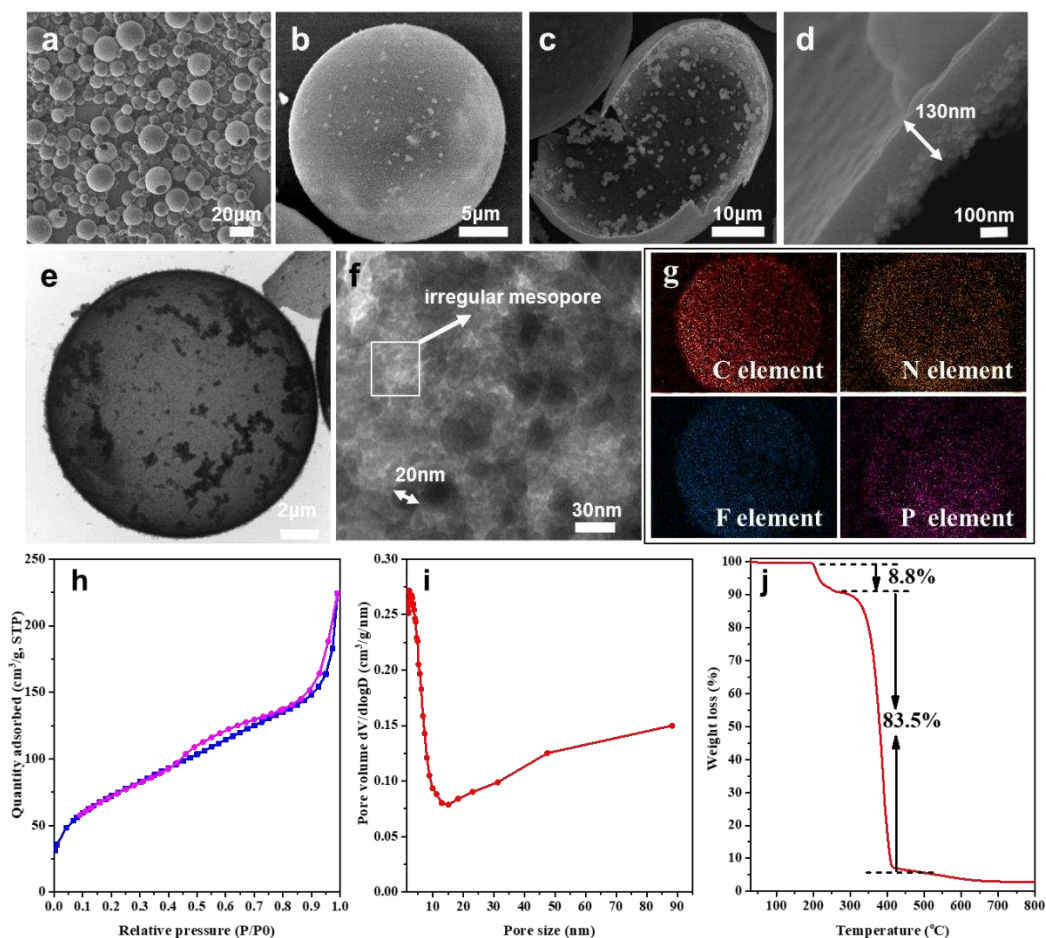
Figure 2. Characterizations of the liquid-solid hybrid capsules (prepared at a shearing speed of 15000 rpm). SEM images of (a) the capsules at low magnification, (b) a single capsule, (c) a single deliberately broken capsule revealing the hollow interior, and (d) a cross-sectional view of the outer crust. TEM images of (e) a single capsule and (f) a segment of the capsule crust. (g) Element mappings of C, N, F and P. (h) Nitrogen adsorption-desorption isotherms of the capsule at 77 K. (i) BJH pore size distribution calculated from the adsorption branch of the isotherm. (j) TG curve.

(Figure 2c). The thickness of the silica curst is approximately 130 nm, as estimated from the cross-sectional image (Figure 2d). Interestingly, two distinct layers were observed to be present on the silica crust. The outer layer was distributed with emulsifier particles and was relatively spongy, while the inner layer was compact. This indicates that the sol-gel process occurs mainly at the inner surfaces of IL droplets. This is because the hydrogen bonding interactions between the hydrolyzed Si-OH and the anion of the IL at the inner interfaces direct the condensation process to occur around the inner surfaces of the droplets, as illustrated in Figure 1B.[44] The spherical structure of the capsules was further confirmed by the TEM image (Figure 2e). A higher level of detail of the microstructures becomes visible from the magnified TEM image (Figure 2f). Irregular pores of a few nanometers are present on the crust. The empty capsules exhibit a type-IV N_2 sorption isotherm with a H4-type hysteresis loop, which is characteristic of a mesoporous structure (Figure 2h). The BET surface area is as high as 266 $m^2 g^{-1}$, which is much higher than that of the silica emulsifier (120 $m^2 g^{-1}$). This high surface area is attributed to the pore formation during the course of the interfacial sol-gel, and the pore size calculated by the BJH method is centered at approximately 2-10 nm, which is in agreement with the TEM observation (Figure 2i). Notably, these pores were generated in the absence of any extra templates. The pore formation may originate from the interfacial sol-gel process in the presence of ILs.[17,44]

Elemental mappings revealed homogeneous distributions of C, N, F and P elements throughout the liquid-solid hybrid material, confirming the successful encapsulation of the IL (Figure 2g). This material was then characterized by TG analysis (Figure 2j). Below 180 °C, no weight loss was observed, indicating a good thermal stability (without decomposition and liquid evaporation). From 180 to 250 °C, there was an 8.8% weight loss, which is attributed to the condensation of silanols on the silica crust. Between 250 and 450 °C, there was a major degree of weight loss up to 83.5%, which is caused by the decomposition of IL. This weight loss is broadly consistent with the elemental analysis results (88.2%). Such a high loading of IL is virtually unattainable for the existing supported liquid phase
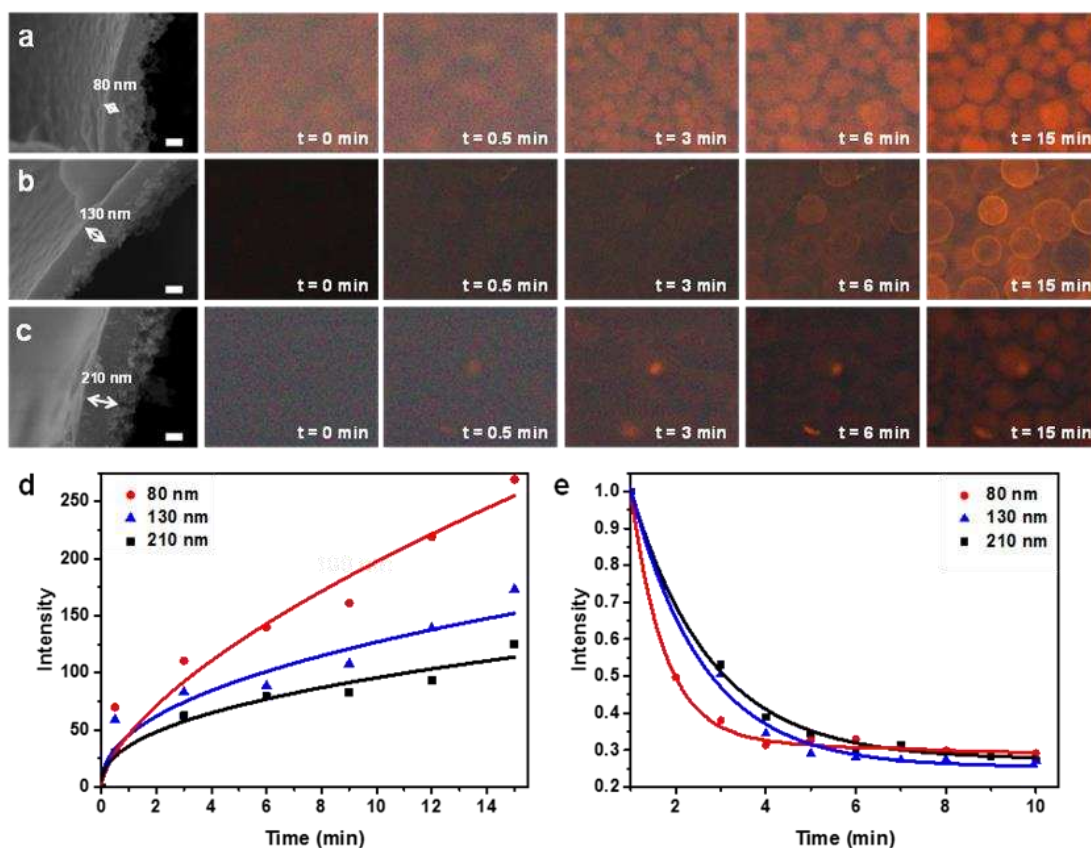
Figure 3. Fluorescence microscopy as a function of time for the diffusion of probe molecules into/out of liquid-solid hybrid capsules with different crust thicknesses. (a)–(c) SEM images showing the cross-sections of silica crusts and series of time-dependent confocal fluorescence microscopy images showing the diffusion of Nile Red (2.5 μM) into the capsules. The crusts were prepared with different TMS amounts, (a) 0.04 g, (b) 0.08 g, (c) 0.12 g, which correspond to average thicknesses of 80, 130 and 210 nm, respectively. Scale bar = 100 nm. (d) Fluorescence intensity as a function of time for the diffusion of Nile Red into hybrid capsules. (e) Fluorescence intensity as a function of time for the diffusion of FITC-I out of the hybrid capsules.

method.[30,45,46] To our knowledge, this is the first production of a crack-free IL-containing capsule. The key to this success is the utilization of unique interfaces and high stability of Pickering emulsions.

2.2. Tuning of the Capsule Size and Crust Thickness. We tuned the capsule size and crust thickness by modifying the synthesis protocol. It is well documented that a higher stirring speed applied during emulsification leads to smaller droplets.[47] When stirring at 5000 rpm, the resultant hybrid capsule was 55±15 μm in size (Figures S3 and S4). When a stirring speed of 15000 rpm was applied, the hybrid capsule size decreased to 28±12 μm. Still, a higher stirring speed of 20000 rpm led to even smaller capsules (16±7 μm). Interestingly, for each sample, the final capsule size was almost the same as its "mother" droplet size, indicating template effects. Moreover, the crust thickness can also be tailored by varying the TMS amount. As Figure S5 shows, upon increasing the amount of TMS from 0.04 to 0.08 and then further to 0.12 g, although the hybrid capsules had a similar morphology and particle diameter, the crust thickness remarkably increased from 80 to 130 and then to 210 nm (see the first panels of Figures 3a-c for their textural parameters and see N_2 sorption characterization in Figure S6). As these results confirmed, our strategy allows the dimensions of the IL pool and the crust thickness to be adjusted in a controlled way.

2.3. Permeability of the Capsules. Fluorescent probes were employed to evaluate the permeability of the hybrid material. A time-dependent fluorescence confocal microscopy (CLSM) image of the hybrid materials was recorded upon addition of a small aliquot of Nile Red-containing solution (Figures 3a-c). For instance, upon contacting the capsule with 80 nm of crust thickness, the fluorescent molecules (initially present outside the hybrid capsule) began to pass through the silica crust and enter the inner IL pool. After only 0.5 min, fluorescent signals were clearly observed inside the IL pool. During the following 3.0-15.0 min, the fluorescent intensity increased gradually as more fluorescent molecules were present in the IL pool (Figure 3d). Meanwhile, to visualize the molecular transport out from the hybrid material, a separate fluorescent experiment was conducted. A fluorescent probe FITC-I was first encapsulated within the hybrid capsule during the preparation (see SI). When the FITC-I-containing hybrid material was dispersed in ethanol (Figures 3e and S7), the fluorescent intensity in the interior IL pool was observed to decline with time, suggesting that the probe molecules diffused out of the capsules. After 4 min, the fluorescent intensity in the IL pool had nearly stabilized. These findings confirm that the outer crust of the material has a good ability to exchange molecules with the surrounding medium.

To determine the impact of the curst thickness on the molecular exchanges, we examined two other hybrid materials with increased crust thicknesses of 130 and 210 nm. The results (Figures 3b-e and S7) showed that the rate of molecular exchanges was correlated with the curst thickness. As the curst thickness increased, the rate decreased due to the increased tortuosity and longer diffusion pathways. This finding can further guide the design of hybrid catalysts with controllable permeability.
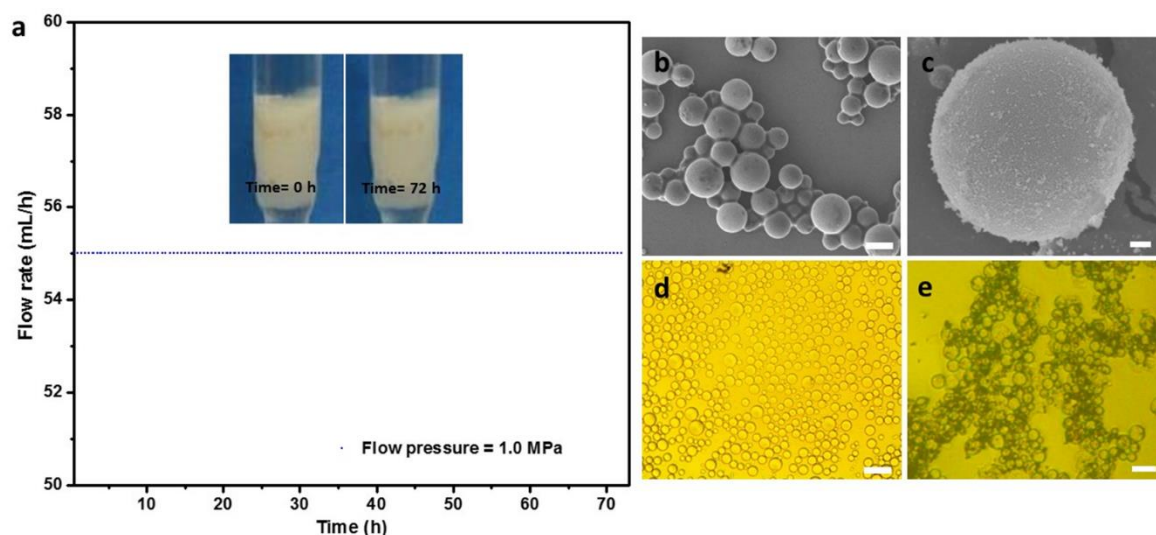
Figure 4. Flow behavior and stability of the liquid-solid hybrid capsules in a column reactor. (a) The flow rate of the mobile phase as a function of time under 1.0 MPa with the inset showing the appearance of the hybrid capsule materials before and after 72 h of continuous flow. (b) and (c) SEM images of the liquid-solid hybrid capsules after 72 h of continuous flow, scale bar = 20 μm for b and 2 μm for c. (d) Microscopic image of the capsules after thermal treatment at 120 °C for 5 h, scale bar = 100 μm. (e) Microscopic image of the capsules after stirring in methanol (30 min), scale bar = 30 μm.

2.4. Mechanical Strength. To examine the mechanical stability, the liquid-solid hybrid material was packed in a fixed-bed reactor. An oil phase at a high velocity (55 mL h⁻¹) was pumped into this reactor under 1.0 MPa. The flow velocity of the eluent from the outlet was monitored. To our satisfaction, over a period of 72 h, the flow velocity remained unchanged (Figure 4a). No leakage of IL was observed, and the height of the packed column did not alter after this treatment (Figure 4a, inset). The capsules remained intact and maintained their structural integrity, as evident by the SEM images (Figures 4b and c). These experiments demonstrate that the hybrid capsules are sufficiently mechanically robust to withstand the flowing liquid even at relatively high flow velocities under pressurized conditions. In contrast, their precursor IL droplets (without growing a silica crust) were observed to flow out from the column when the applied pressure was above 0.3 MPa (Figure S8). The high stability against mechanical compression is attributed to the unique structure, where the inner IL pool supports the silica crust when there is external stress. Moreover, the hybrid capsules can withstand thermal treatment and tolerate polar solvents, significantly beyond the stability exhibited by the Pickering emulsion droplets (Figures S9 and S10). As Figures 4d and e show, after 5 h of thermal treatment at 120 °C or treatment with methanol under stirring, the structural integrity of the capsules was still well preserved.

2.5. Kinetic Resolution of Alcohols in the Continuous Flow System. Based on the above results, we then examined the liquid-solid hybrid catalyst in continuous flow reactions. We first chose an enzyme to investigate because it is highly used within the IL field for various organic transformations.[37,48] Following the above procedure, a lipase CALB was trapped within the capsules by adding a given amount of CALB before formulating the Pickering emulsions. To check the distribution of CALB within the IL pool, we labeled CALB with a fluorescent probe, Rhodamine B. The fluorescence-labeled CALB was homogeneously distributed inside the IL pool, as judged from the fluorescent signals (Figure S11). No fluorescent signals were found outside the capsules, which is indicative of the quantitative entrapment of CALB.

The kinetic resolution of the alcohol catalyzed by CALB, which is an important method to produce chiral alcohols and esters, was examined.[49,50] Being micron-sized microspheres, the CALB-containing hybrid catalyst could be directly packed in a fixed-bed column reactor, as anticipated. A solution of racemic 1-phenylethyl alcohol and vinyl acetate (acylation reagent) in octane was fed from the inlet of the reactor, and the product-containing stream was collected on the outlet side. Notably, the concentrations of these two reactants of as high as 0.35 and 1.40 M were applied here. Such high reaction concentrations are impossible in our previously reported Pickering emulsion system since
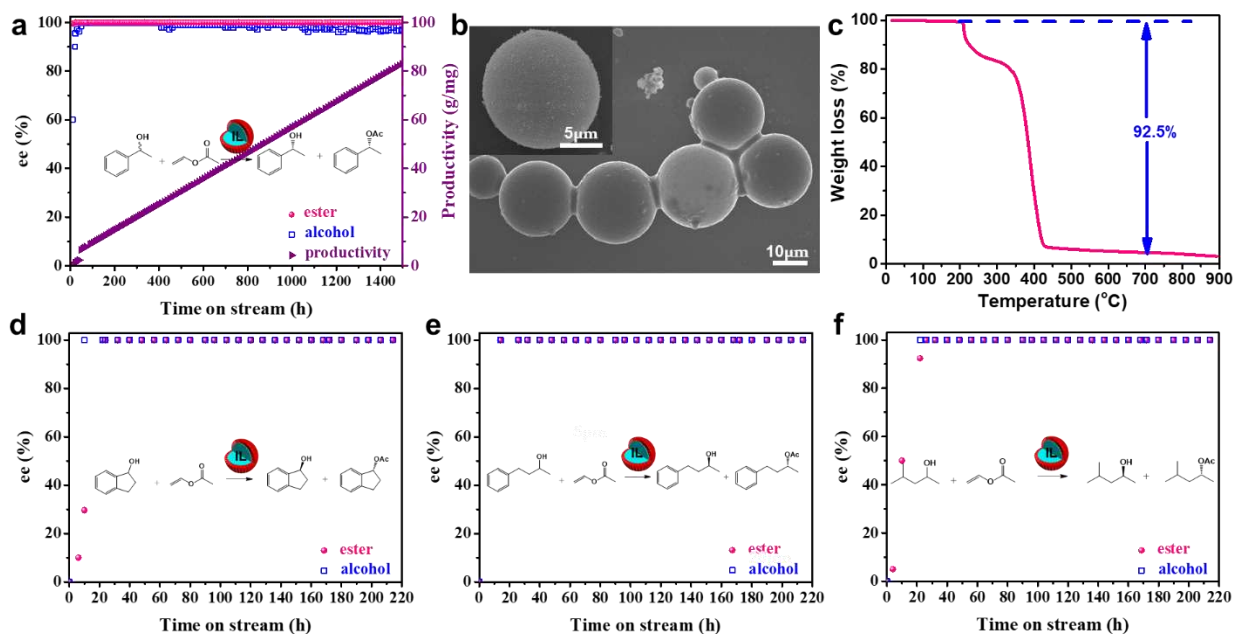
Figure 5. CALB-catalyzed kinetic resolution of the alcohols over the liquid-solid hybrid catalyst-based continuous flow system. Pink points represent the yielded ester, blue points represent the alcohol product, and purple points represent productivity (grams of the converted substrate per enzyme). (a) 1-Phenylethyl alcohol as the substrate. (b) SEM images of the catalyst after 1500 h of continuous flow reaction. (c) TG curve of the catalyst after 1500 h of continuous flow reaction. Different alcohols as the substrate: (d) 1-indanol, (e) 4-phenyl-2-butanol, (f) 4-methyl-2-pentanol. Reaction conditions: 5.0 g of liquid-solid hybrid material (CALB concentration, 0.64 mg g⁻¹), a solution of racemic alcohol (0.35 M) and vinyl acetate (1.40 M) in octane as the mobile phase, 45 °C, 2.3~2 mL h⁻¹ (a) and 1 mL h⁻¹ (d, e and f).

concentrated polar substrates cause breakage of droplets. The enantiomeric excesses (ee values) of the alcohol and the produced ester are plotted as a function of time in Figure 5a. The ee values of the two compounds rapidly increased to 99%. Impressively, these high ee values were well maintained over 1500 h on stream although the flow velocity was adjusted from the initial 2.3 mL h^{-1} to the final value of 2.0 mL h^{-1}. The results confirm the long-term stability of our liquid-solid hybrid catalyst in the continuous flow system. After this long period of time, the morphology and size of the capsules were found to be virtually unchanged, as shown in the SEM image (Figure 5b). No significant loss of IL occurred, which was supported by the TG analysis of the spent catalyst (Figure 5c, an IL loss of approximately 6.3 wt% was observed compared with the above fresh catalyst, based on the weight loss between 200-300 °C). The good preservation of the IL within the capsules should be attributed to the combination of the confinement arising from the silica crusts and the immiscibility of IL with the mobile oil phase. The CALB productivity (grams of product per mg enzyme) was found to increase linearly with time (Figure 5a). The productivity was estimated to be as high as 83.6 g mg^{-1} after 1500 h. Therefore, 1 g of enzyme can resolve 83.6 kg of racemic 1-phenylethyl alcohol, highlighting the extremely high level of productivity.[51] Moreover, for other substrates, such as racemic 1-indanol, 4-phenyl-2-butanol and 4-methyl-2-pentanol, the ee values of the corresponding alcohols and esters were also maintained at 99% over 220 h (Figures 5d, e and f), confirming the good substrate scope.

To benchmark the catalytic activity of the hybrid catalyst, we compared it to CALB in a batch system that represents a homogeneous catalysis reaction. To determine the kinetic parameters of CALB in these two systems, different concentrations of 1-phenylethyl alcohol (from 0.05 to 0.5 M) were applied (Figures 6a and S12). For the homogeneous system with 0.05 M alcohol, the ee value of 1-phenylethyl alcohol that was achieved after 60 min was only 6.1%. The ee value showed no further increase after 60 min, which was caused by the usual strong product inhibition effect.[52,53] The specific activity of CALB was estimated to be 0.16 U mg^{-1}. In contrast, the hybrid catalyst in the continuous flow system produced ee values of approx. 64% at the steady state, and the specific activity was estimated to be 2.04 U mg^{-1}. This is a 12.8-fold enhancement compared with the homogeneous system. Such a striking enhancement was also observed at other concentrations (Figure S12). Based on these results at different concentrations, we calculated the kinetic parameters of CALB in these two systems, including the apparent Michaelis-Menten constant, k_m (affinity of enzyme to the substrate), the maximal reaction rate, V_{max} (the reaction rate when the active sites are saturated with substrate) and the turnover number, k_{cat} (see Figure S13). As displayed in Figure 6b, the k_m for the

flow system was calculated to be 0.11 M, whereas the k_m for the conventional biphasic system was 0.05 M. Although different, they are still close, indicating that the enzyme in these two systems shares a similar microenvironment. However, the V_{max} in the flow system was 3.2×10^{-3} M min^{-1}, which was 26.0-fold higher than that in the homogeneous system (1.23×10^{-4} M min^{-1}). Additionally, the k_{cat} in the flow system was 26.4-fold higher than that for the homogeneous reaction. The significant decrease in product inhibition arising from timely and efficient removal of the product from the flow reaction system may be one main causes of the enhancements.

A crucial factor in realizing the efficient exchange of molecules may be the huge reaction areas created by the micron-sized capsules. To corroborate this, we investigated the impact of the capsule size on the catalysis efficiency. As shown in Figures 6 (c$_1$ and c$_2$), under exactly the same conditions, the ee values of the alcohol at the steady state differ considerably, depending on the capsule size. As the capsule size increased from 16±7 to 28±12 and to 55±15 μm, the ee value of the alcohol at steady state decreased from 89 to 56 and to 16%, while the corresponding specific activity of the enzyme decreased from 5.65 to 3.30 and to 1.01 U mg^{-1}. The observed specific activity as a function of the capsule size can be explained in terms of the surface area and diffusion distance. Increasing the capsule size results in a decrease in the interface area and an increase in the diffusion distance to reach the interior of the IL pool. Moreover, the crust thickness also influences the observed specific activity. As the crust thickness decreased from 210 to 130 and to 80 nm, the ee value of the alcohol at steady state significantly increased (Figures 6, d$_1$ and d$_2$), and the observed specific activity increased from 1.27 to 3.30 and finally 5.40 U mg^{-1}. This increase is attributed to the improved permeability resulting from the decreased tortuosity, which is in agreement with our aforementioned fluorescent experimental results.

Furthermore, the CALB specific activity was related to its loading in the liquid-solid hybrid catalyst (Figures 6, e$_1$ and e$_2$). By varying the amount of CALB introduced, its loading was steadily tuned upward from 0.08 to 0.64 mg g^{-1}. Upon increasing the enzyme loading, the ee values of the alcohol increased from 37.5% to 98.5%, while the observed specific activities decreased from 5.51 to 1.38 U mg^{-1}. To rationalize these results, we established a theoretical model (more details are included in SI). Under steady state conditions, the amount of product C generated within an IL pool will be the same as the amount coming out of it, namely:

$$-4\pi R^2 D_{IL}^C \left.\frac{\partial C}{\partial r}\right|_{R^-} = -4\pi R^2 D_O^C \left.\frac{\partial C}{\partial r}\right|_{R^+} \tag{1}$$

where R is the radius of the IL pool, r is the radial distance from the center of the IL pool, C represents concentration of the product C, D_{IL}^C and D_O^C are the diffusion coefficients of product C in the dispersed IL
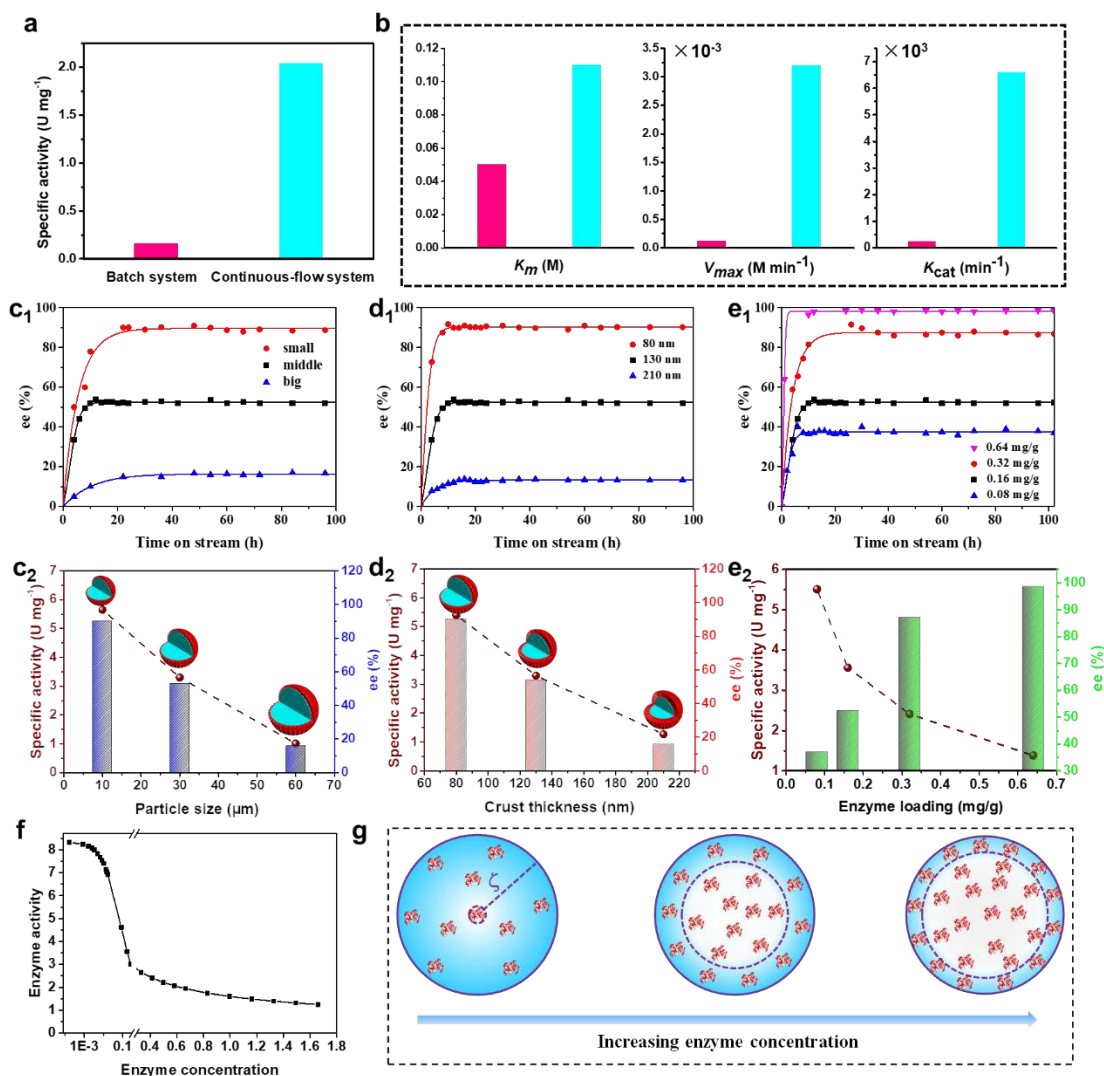
**Figure 6.** Kinetic resolution of 1-phenylethyl alcohol over the liquid-solid hybrid catalyst in continuous flow systems or over CALB in biphasic batch systems. The specific activity (U mg⁻¹) is expressed as *μ*mol of substrate converted per min per mg enzyme (i.e., *μ*mol min⁻¹ mg⁻¹). The specific activity for the batch reaction was calculated over the first 20 min, and that for the flow reaction was calculated at steady state. (a) Comparison of the continuous flow (magenta) and batch (cyan) reactions using a concentration of 0.05 M for 1-phenylethyl alcohol. (b) K_m, V_{max} and k_{cat} for CALB in the liquid-solid hybrid catalyst-based continuous flow system and in the batch reaction system. Batch reaction conditions are included in Figure S12. Continuous flow reactions conditions: 1.0 g liquid-solid hybrid catalyst (CALB loading, 0.16 mg g⁻¹), 1-phenylethyl alcohol (0.05, 0.10, 0.30 or 0.50 M), vinyl acetate (0.2, 0.40, 1.20 and 2.00 M) in *n*-octane, 45 °C, 1.2 mL h⁻¹. (c) Comparison of the kinetic resolution of alcohols over different-sized liquid-solid hybrid catalysts (c_1, alcohol ee values with time; c_2, their specific activity). The reaction conditions were the same as in b except that the mobile phase was a solution of 1-phenylethyl alcohol (0.10 M) and vinyl acetate (0.40 M). (d) Comparison of the kinetic resolution of alcohols over the liquid-solid hybrid catalysts with different crust thicknesses (d_1, alcohol ee values with time; d_2, their specific activity). The reaction conditions were the same as in c. (e) Comparison of the kinetic resolution of the alcohols over the liquid-solid hybrid catalysts with different enzyme loadings (e_1, alcohol ee values with time; e_2, their specific activity). The reaction conditions were the same as in c. (f) Theoretical results of the enzyme activity as a function of the enzyme loadings. (g) Illustration of the variation of reaction region ζ (represented by the distance from boundary to inner dashed line) with increasing enzyme loadings.

phase and continuous oil phase, and R^- and R^+ refer to points infinitely close to the internal and external IL pool surface respectively. Then, by substituting the results for the variation of C with r in and out of the IL pool (see SI), the rate of the generated product per IL pool was calculated to be

$$-4\pi R^2 D_{IL}^C \frac{\partial C}{\partial r}\bigg|_{R^-} = 8\pi n D_{IL}^C \left[\sinh(R/\zeta) - \frac{R}{\zeta}\cosh(R/\zeta) \right] \quad (2)$$

where n is the integration constant, the value of which was obtained by considering the boundary conditions at

H

the interface of the IL pool, at its center and far away from it (also see SI), and ζ represents a length scale of the reaction region thickness. Then, the rate of product generated inside an IL pool can be expressed as per amount of enzyme contained within the same IL pool, leading to the theoretical enzyme activity (or T_{ea} for short). With the appropriate value of n substituted in (2) we arrive at:

$$T_{ea} = \frac{3D_o^A}{R^2 C_{ez}}\left[A_o^0 - \frac{\left(D_o^A A_o^0 + D_o^c C_o^0\right)\left(1 - \frac{K_1 B_{IL}^0 \zeta^2}{D_{IL}^A}\right)}{D_o^A\left(1 - \frac{K_1 B_{IL}^0 \zeta^2}{D_{IL}^A}\right) + D_o^c \frac{\alpha_A}{\alpha_C}\frac{K_1 B_{IL}^0 \zeta^2}{D_{IL}^c}}\right] \quad (3)$$

In this equation, C_{ez} is the concentration of the enzyme, D_O^A and D_{IL}^A are diffusion coefficients of substrate A in oil and IL, respectively, A_O^0, B_O^0 and C_O^0 and A_{IL}^0, B_{IL}^0 and C_{IL}^0 are the concentrations of substrates A, B and product C in oil at distances far from the IL pool and in the IL phase, K_1 and K_2 are the rate constant of the forward and backward reaction in IL, α_A and α_C are the partition constants of A and C between IL and oil phases. Specifically, as a crucial prediction of this theory, ζ is calculated to be $\zeta^{-2} = \frac{K_1 B_{IL}^0}{D_{IL}^A} + \frac{K_2}{D_{IL}^C}$. It is now reasonable that both K_1 and K_2 increase in proportion with C_{ez}, whereas $\zeta \propto 1/\sqrt{C_{ez}}$ (as seen from the above equation). Hence, although the rate of reaction is increased by addition of more enzyme, when R > ζ, the reaction becomes constrained in a smaller, more confined volume inside the IL pool. For a given reaction system, after substituting the appropriate numerical values for various parameters into equation (3), the enzyme activity as a function of enzyme concentration can be plotted, as shown in Figure 6f. The theoretical enzyme activity significantly decreases with increased enzyme loading and then decreases slowly at high loadings,
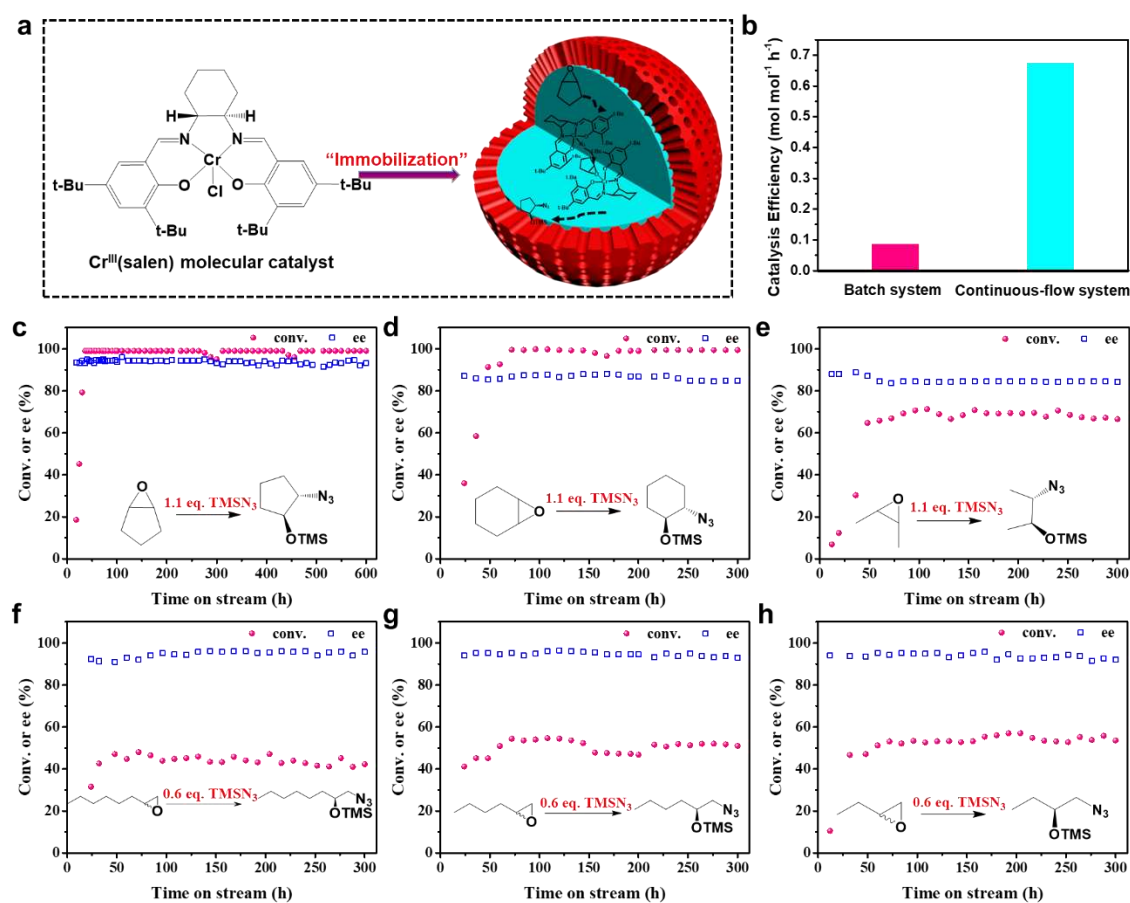

Figure 7. The ARO reactions of different epoxides over the liquid-solid hybrid catalyst in the continuous flow system or Cr^III(salen)-based batch system. (a) Molecular structure of the Cr^III(salen) catalyst and its corresponding liquid-solid hybrid catalyst. (b) Comparison of the catalysis efficiencies in the continuous flow and batch systems using cyclopentene oxide as a substrate. Reactions with different epoxides: (c) cyclopentene oxide, (d) cyclohexene oxide, (e) 2,3-epoxybutane, (f) 1,2-epoxyoctane, (g) 1,2-epoxyhexane and (h) 1,2-epoxybutane. Pink points are epoxide conversions, and blue points are ee values of azido silyl ether products. The liquid-solid hybrid catalyst consists of 4.5 g [BMIM]PF_6, 1.2 g [BMIM]BF_4 and 45 mg Cr^III(salen). Reaction conditions: epoxide (0.04 M) and TMSN_3 (0.0.044 or 0.024 M) in *n*-octane, room temperature, 0.6-1.2 mL h^-1.

I

which is consistent with the experimental results. Such a change is understandable in terms of the diffusion-reaction process occurring inside the IL pool. As the enzyme loading was increased, ζ became progressively smaller (Figure 6g). Thus, only a portion of the enzymes took part in the reaction, and the rest closer to the center of the IL pool were idle because the slow diffusion limits the timely supply of substrates to the more inner parts of the IL pool. In contrast, at low enzyme loadings, ζ was larger than the IL pool size. This means all enzymes in the entire body of the pool take part in the reactions, leading to an optimum value for special activity. The experimental and theoretic findings both suggest that there is still a diffusion effect underlying the working conditions of the continuous flow catalysis reactor, despite the homogeneous microenvironment. Importantly, the consistency between experimental and theoretical results implies that the catalytic performance of the hybrid catalyst is predictable and even rationally designed.

Taken together, as the above experimental and theoretical results corroborated, our strategy allows the catalysis efficiency of the hybrid catalyst to be finely tuned via rational engineering of the dimension of the IL droplets, the crust thickness and the enzyme loading. These merits are inaccessible for homogeneous or heterogeneous catalysts alone and are unachievable for existing methods.

2.6. Asymmetric Ring Opening (ARO) of Epoxides in the Continuous Flow System. We then checked the applicability of our method to homogeneous molecular catalysts. For instance, Cr^{III}(salen)-catalyzed ARO of an epoxide with trimethylsilyl azide (TMSN$_3$), a typical asymmetric reaction, was investigated.[54] Using the procedure described above, Cr^{III}(salen) molecules were "trapped" within the IL pool of the hybrid catalyst (Figure 7a). In a batch reaction, a 19.7% conversion of cyclopentene oxide was afforded within 12 h (kinetic plots are provided in Figure S14). The catalysis efficiency (moles of converted reactants per mole of catalyst per h) was calculated to be 0.0865 mol mol^{-1} h^{-1} (Figure 7b). In contrast, in the hybrid catalyst-based continuous flow system, full conversion was achieved at steady state, and the catalysis efficiency was 0.674 mol mol^{-1} h^{-1}, which is 7.8-fold higher than that of the batch reaction. Additionally, the greater than 99% conversion and 93% enantioselectivity were well maintained even after a period of 600 h (Figure 7c). The total TON was as high as 337 mol mol^{-1}, which has been difficult to achieve for previously reported systems.[55,56] For other epoxides, the hybrid catalyst also worked well (Figures 7d-h). Cyclohexene oxide was completely converted and the ee values of the generated azido silyl ether were maintained at 85~88% over a time of 300 h on stream. For 2,3-epoxybutane, 66~70% conversions and 84~88% ee values were obtained. Apart from *meso*-epoxides, the

ARO reactions over the hybrid catalyst can be further extended to terminal epoxides, such as 1,2-epoxyoctane, 1,2-epoxyhexane and 1,2-epoxybutane. For these substrates, conversions of approximately 45%, 51% and 53% were maintained over a period of 300 h (the theoretical maximum conversions were approx. 50% for these substrates[54]), and corresponding ee values were approximately 94-96%, 93-95% and 92-95%. After continuous running of 300 h, the conversions and enantioselectivities showed no apparent decrease. These results constitute additional proof for the effectiveness of our strategy in dealing with homogeneous catalysts.

2.7. Tsuji-Trost Reactions in the Continuous Flow System. To further examine the generality of the concept, the palladium-catalyzed Tsuji-Trost reaction which is often used to construct C-heteroatom bonds was investigated.[57,58] The molecular catalyst [Pd(OAc)$_2$] and the ligand, TPPTS [(triphenyl phosphine-3,3',3"-trisulfonic acid trisodium salt)], were co-trapped within the IL pool of the hybrid catalyst according to the above procedure (Figure S15a). The prepared catalyst likewise showed high activity and long-term stability in the allylic substitution of (*E*)-1, 3-diphenylallyl acetate with morpholine or piperidine as N-nucleophiles. Compared with the batch reaction counterparts, the continuous flow system exhibited enhanced catalysis efficiency (3.60 *vs.* 2.23 mol mol^{-1} h^{-1}; see kinetic plots in Figure S15b). The conversions of (*E*)-1, 3-diphenylallyl acetate at steady state were more than 99% over a period of 800 h, and the total TON reached up to 2640 mol mol^{-1} (Figures S15c, d). Notably, almost no Pd or TPPTS were detected in the effluent. This may be attributed to the strong interactions between the Pd/TPPTS and the IL surroundings, keeping the former securely within the capsules. These results once again consolidate the generality and adaptability of the method proposed in this work.

3. CONCLUSION

We successfully developed a Pickering emulsion method to prepare a liquid-solid hybrid catalyst, which allowed us to overcome the limitations of the existing methods and efficiently bridge the gaps between homogeneous and heterogeneous catalysis in an unprecedented manner. As a hybrid homogeneous and heterogeneous catalyst, this type of catalyst consists of a crack-free permeable silica outer crust and an IL pool, which was confirmed to be powerful for hosting enzymes and homogeneous molecular catalysts. The thickness and permeability of the crust and the dimensions of the inner IL pool are highly tunable. Crucially, the hybrid catalyst not only has a homogeneous catalytic environment but is also amenable to continuous flow catalysis. As exemplified by the enzymatic kinetic resolution of alcohols, the catalysis efficiency was improved by over an order of magnitude compared with

batch homogeneous counterparts due to enabling of the continuous flow. Impressively, the catalysis efficiency and selectivity showed no significant decrease over 1500 h. The Cr^{III}(salen)-catalyzed asymmetric ring opening of the epoxides and the Pd-catalyzed Tsuji-Trost allylic substitution reaction further corroborated the versatility and adaptability of our method in dealing with homogeneous catalysts. Furthermore, their catalytic performances can be regulated by rationally engineering the catalyst structure. We believe that our method provides a new direction for filling the gap between homogeneous, heterogeneous and biological catalysis and brings new opportunities for practical applications of enzymes and homogeneous catalysts.

ASSOCIATED CONTENT

Supporting Information

Experimental details; TEM images; Water contact angles; Optical microscopy images; SEM images; Confocal fluorescence microscopy images; Appearance of the Pickering emulsions; Theoretical investigation; Equation derivation process; Reaction kinetics monitoring; MS and NMR data for products. This material is available free of charge via the Internet at http://pubs.acs.org.

AUTHOR INFORMATION

Corresponding Author

*hqyang@sxu.edu.cn

Author Contributions

§These authors contributed equally.

Notes

The authors declare no competing financial interests.

ACKNOWLEDGMENT

REFERENCES

(1) Copéret, C.; Chabanas, M.; Saint-Arroman, R. P.; Basset, J. M. Homogeneous and Heterogeneous Catalysis: Bridging the Gap through Surface Organometallic Chemistry. *Angew. Chem., Int. Ed.* 2003, 42, 156–181.

(2) Li, C.; Liu, Y. *Bridging Heterogeneous and Homogeneous Catalysis: Concepts, Strategies, and Applications.* Wiley–VCH, Weinheim, Germany, 2014.

(3) Gross, E.; Somorjai, G. A. Mesoscale Nanostructures as a Bridge between Homogeneous and Heterogeneous Catalysis. *Top. Catal.* 2014, 57, 812–821.

(4) Corma, A. Heterogeneous Catalysis: Understanding for Designing, and Designing for Applications. *Angew. Chem., Int. Ed.* 2016, 55, 6112–6113.

(5) Gross, E.; Liu, J. H. C.; Toste, F. D.; Somorjai, G. A. Control of Selectivity in Heterogeneous Catalysis by Tuning Nanoparticle Properties and Reactor Residence Time. *Nat. Chem.* 2012, 4, 947–952.

(6) Atodiresei, L.; Vila, C.; Rueping, M. Asymmetric Organocatalysis in Continuous Flow: Opportunities for Impacting Industrial Catalysis. *ACS Catal.* 2015, 5, 1972–1985.

(7) Tsubogo, T.; Oyamada, H.; Kobayashi, S. Multistep Continuous–Flow Synthesis of (R)– and (S)–Rolipram Using Heterogeneous Catalysts. *Nature*, 2015, 520, 329–332.

(8) Zhao, D. B.; Ding, K. L. Recent Advances in Asymmetric Catalysis in Flow. *ACS Catal.* 2013, 3, 928–944.

(9) Sun, Q.; Dai, Z. F.; Meng, X. J.; Wang, L.; Xiao, F. S. Task–Specific Design of Porous Polymer Heterogeneous Catalysts beyond Homogeneous Counterparts. *ACS Catal.* 2015, 5, 4556–4567.

(10) García-Verdugo, E.; Altava, B.; Burguete, M. I.; Lozano, P.; Luis, S. V. Ionic Liquids and Continuous Flow Processes: A Good Marriage to Design Sustainable Processes. *Green Chem.* 2015, 17, 2693–2713.

(11) Crossley, S.; Faria, J.; Shen, M.; Resasco, D. E. Solid Nanoparticles that Catalyze Biofuel Upgrade Reactions at the Water/Oil Interface. *Science* 2010, 327, 68–72.

(12) Pera-Titus, M.; Leclercq, L.; Clacens, J. M.; De Campo, F.; Nardello-Rataj, V. Pickering Interfacial Catalysis for Biphasic Systems: From Emulsion Design to Green Reactions. *Angew. Chem., Int. Ed.* 2015, 54, 2006–2021.

(13) Drake, T.; Ji, P. F.; Lin, W. B. Site Isolation in Metal–Organic Frameworks Enables Novel Transition Metal Catalysis. *Acc. Chem. Res.* 2018, 51, 2129–2138.

(14) Wang, A. Q.; Li, J.; Zhang, T. Heterogeneous Single–Atom Catalysis. *Nat. Rev. Chem.* 2018, 2, 65–81.

(15) Kang, X. C.; Zhang, J. L.; Shang, W. T.; Wu, T. B.; Zhang, P.; Han, B. X.; Wu, Z. H.; Mo, G.; Xing, X. Q. One–Step Synthesis of Highly Efficient Nanocatalysts on the Supports with Hierarchical Pores Using Porous Ionic Liquid–Water Gel. *J. Am. Chem. Soc.* 2014, 136, 3768–3771.

(16) Cole-Hamilton, D. J. Homogeneous Catalysis–New Approaches to Catalyst Separation, Recovery, and Recycling. *Science* 2003, 299, 1702–1706.

(17) Su, Q.; Qi, Y. Q.; Yao, X. Q.; Cheng, W. G.; Dong, L.; Chen, S. S.; Zhang, S. J. Ionic Liquids Tailored and Confined by One–Step Assembly with Mesoporous Silica for Boosting the Catalytic Conversion of CO_2 into Cyclic Carbonates. *Green Chem.* 2018, 20, 3232–3241.

(18) Taccardi, N.; Grabau, M.; Debuschewitz, J.; Distaso, M.; Brandl, M.; Hock, R.; Maier, F.; Papp, C.; Erhard, J.; Neiss, C.; Peukert, W.; Görling, A.; Steinrück, H. P.; Wasserscheid, P. Gallium–Rich Pd–Ga Phases as Supported Liquid Metal Catalysts. *Nat. Chem.* 2017, 9, 862–867.

(19) Heitbaum, M.; Glorius, F.; Escher, I. Asymmetric Heterogeneous Catalysis. *Angew. Chem., Int. Ed.* 2006, 45, 4732–4762.

(20) McMorn, P.; Hutchings, G. J. Heterogeneous Enantioselective Catalysts: Strategies for the Immobilisation of Homogeneous Catalysts. *Chem. Soc. Rev.* 2004, 33, 108–122.

(21) Yang, Q. H.; Han, D. F.; Yang, H. Q.; Li, C. Asymmetric Catalysis with Metal Complexes in Nanoreactors. *Chem. Asian J.* 2008, 3, 1214–1229.

(22) Kreituss, I.; Bode, J. W. Flow Chemistry and Polymer–Supported Pseudoenantiomeric Acylating Agents Enable Parallel Kinetic Resolution of Chiral Saturated N–Heterocycles. *Nat. Chem.* 2017, 9, 446–452.

(23) Zhao, Y. P.; Zhang, X. M.; Sanjeevi, J.; Yang, Q. H. Hydroformylation of 1-Octene in Pickering Emulsion Constructed by Amphiphilic Mesoporous Silica Nanoparticles. *J. Catal.* 2016, 334, 52–59.

(24) Barbaro, P.; Liguori, F. Ion Exchange Resins: Catalyst Recovery and Recycle. *Chem. Rev.* 2009, 109, 515–529.

(25) Dergunov, S. A.; Khabiyev, A. T.; Shmakov, S. N.; Kim, M. D.; Ehterami, N.; Weiss, M. C.; Birman, V. B.; Pinkhassik, E. Encapsulation of Homogeneous Catalysts in Porous Polymer Nanocapsules Produces Fast–Acting Selective Nanoreactors. *ACS Nano* **2016**, 10, 11397–11406.

(26) Alamillo, R.; Crisci, A. J.; Gallo, J. M. R.; Scott, S. L.; Dumesic, J. A. Tailored Microenvironment for Catalytic Biomass Conversion in Inorganic–Organic Nanoreactors. *Angew. Chem., Int. Ed.* **2013**, 52, 10349–10351.

(27) Long, J.; Liu, G. H.; Cheng, T. Y.; Yao, H.; Qian, Q. Q.; Zhuang, J. L.; Gao, F.; Li, H. X. Immobilization of Rhodium–Based Transfer Hydrogenation Catalysts on Mesoporous Silica Materials. *J. Catal.* **2013**, 298, 41–50.

(28) An, Z.; Guo, Y.; Zhao, L. W.; Li, Z.; He, J. L–Proline–Grafted Mesoporous Silica with Alternating Hydrophobic and Hydrophilic Blocks to Promote Direct Asymmetric Aldol and Knoevenagel–Michael Cascade Reactions. *ACS Catal.* **2014**, 4, 2566–2576.

(29) Arhancet, J. P.; Davis, M. E.; Merola, J. S.; Hanson, B. E. Hydroformylation by Supported Aqueous–Phase Catalysis: A New Class of Heterogeneous Catalysts. *Nature* **1989**, 339, 454–455.

(30) Zhao, J.; Gu, S. C.; Xu, X. L.; Zhang, T. T.; Yu, Y.; Di, X. X.; Ni, J.; Pan, Z. Y.; Li, X. N. Supported Ionic–Liquid–Phase–Stabilized Au(III) Catalyst for Acetylene Hydrochlorination. *Catal. Sci. Technol.* **2016**, 6, 3263–3270.

(31) Vishwakarma, N. K.; Singh, A. K.; Hwang, Y. H.; Ko, D. H.; Kim, J. O.; Babu, A. G.; Kim, D. P. Integrated CO_2 Capture–Fixation Chemistry via Interfacial Ionic Liquid Catalyst in Laminar Gas/Liquid Flow. *Nat. Commun.* **2017**, 8, 14676.

(32) Brünig, J.; Csendes, Z.; Weber, S.; Gorgas, N.; Bittner, R. W.; Limbeck, A.; Bica, K.; Hoffmann, H.; Kirchner, K. Chemoselective Supported Ionic–Liquid–Phase (SILP) Aldehyde Hydrogenation Catalyzed by an Fe(II) PNP Pincer Complex. *ACS Catal.* **2018**, 8, 1048–1051.

(33) Weiss, E.; Dutta, B.; Kirschning, A.; Abu-Reziq, R. BMIm-PF_6@SiO_2 Microcapsules: Particulated Ionic Liquid as a New Material for the Heterogenization of Catalysts. *Chem. Mater.* **2014**, 26, 4781–4787.

(34) Palomar, J.; Lemus, J.; Alonso-Morales, N.; Bedia, J.; Gilarranz, M. A.; Rodriguez, J. J. Encapsulated Ionic Liquids (ENILs): From Continuous to Discrete Liquid Phase. *Chem. Commun.* **2012**, 48, 10046–10048.

(35) Shi, F.; Zhang, Q. H.; Li, D. M.; Deng, Y. Q. Silica-Gel-Confined Ionic Liquids: A New Attempt for the Development of Supported Nanoliquid Catalysis. *Chem. Eur. J.* **2005**, 11, 5279–5288.

(36) Zhang, M.; Wei, L. J.; Chen, H.; Du, Z. P.; Binks, B. P.; Yang, H. Q. Compartmentalized Droplets for Continuous Flow Liquid–Liquid Interface Catalysis. *J. Am. Chem. Soc.* **2016**, 138, 10173–10183.

(37) Zhang, M.; Ettelaie, R.; Yan, T.; Zhang, S. J.; Cheng, F. Q.; Binks, B. P.; Yang, H. Q. Ionic Liquid Droplet Microreactor for Catalysis Reactions Not at Equilibrium. *J. Am. Chem. Soc.* **2017**, 139, 17387–17396.

(38) Hallett, J. P.; Welton, T. Room–Temperature Ionic Liquids: Solvents for Synthesis and Catalysis. *Chem. Rev.* **2011**, 111, 3508–3576.

(39) Zhang, Q. H.; Zhang, S. G.; Deng, Y. Q. Recent Advances in Ionic Liquid Catalysis. *Green Chem.* **2011**, 13, 2619–2637.

(40) Jiang, H.; Hong, L. Z.; Li, Y. X.; Ngai, T. All–Silica Submicrometer Colloidosomes for Cargo Protection and Tunable Release. *Angew. Chem., Int. Ed.* **2018**, 57, 11662–11666.

(41) Binks, B. P.; Dyab, A. K. F.; Fletcher, P. D. I. Contact Angles in Relation to Emulsions Stabilised Solely by Silica Nanoparticles Including Systems Containing Room Temperature Ionic Liquids. *Phys. Chem. Chem. Phys.* **2007**, 9, 6391–6397.

(42) Aveyard, R.; Binks, B. P.; Clint, J. H. Emulsions Stabilised Solely by Colloidal Particles. *Adv. Colloid Interface Sci.* **2003**, 100–102, 503–546.

(43) Li, M.; Harbron, R. L.; Weaver, J. V. M.; Binks, B. P.; Mann, S. Electrostatically Gated Membrane Permeability in Inorganic Protocells. *Nat. Chem.* **2013**, 5, 529–536.

(44) Zhou, Y.; Schattka, J. H.; Antonietti, M. Room–Temperature Ionic Liquids as Template to Monolithic Mesoporous Silica with Wormlike Pores via a Sol–Gel Nanocasting Technique. *Nano Lett.* **2004**, 4, 477–481.

(45) Sun, J. K.; Antonietti, M.; Yuan, J. Y. Nanoporous Ionic Organic Networks: From Synthesis to Materials Applications. *Chem. Soc. Rev.* **2016**, 45, 6627–6656.

(46) Luza, L.; Rambor, C. P.; Gual, A.; Bernardi, F.; Domingos, J. B.; Grehl, T.; Brüner, P.; Dupont, J. Catalytically Active Membranelike Devices: Ionic Liquid Hybrid Organosilicas Decorated with Palladium Nanoparticles. *ACS Catal.* **2016**, 6, 6478–6486.

(47) Thompson, K. L.; Armes, S. P.; York, D. W. Preparation of Pickering Emulsions and Colloidosomes with Relatively Narrow Size Distributions by Stirred Cell Membrane Emulsification. *Langmuir* **2011**, 27, 2357–2363.

(48) Itoh, T. Ionic Liquids as Tool to Improve Enzymatic Organic Synthesis. *Chem. Rev.* **2017**, 117, 10567–10607.

(49) Verho, O.; Bäckvall, J. E. Chemoenzymatic Dynamic Kinetic Resolution: A Powerful Tool for the Preparation of Enantiomerically Pure Alcohols and Amines. *J. Am. Chem. Soc.* **2015**, 137, 3996–4009.

(50) Koeller, K. M.; Wong, C. H. Enzymes for Chemical Synthesis. *Nature* **2001**, 409, 232–240.

(51) Pushpanath, A.; Siirola, E.; Bornadel, A.; Woodlock, D.; Schell, U. Understanding and Overcoming the Limitations of *Bacillus badius and Caldalkalibacillus thermarum* Amine Dehydrogenases for Biocatalytic Reductive Amination. *ACS Catal.* **2017**, 7, 3204–3209.

(52) Sandig, B.; Buchmeiser, M. R. Highly Productive and Enantioselective Enzyme Catalysis under Continuous Supported Liquid–Liquid Conditions Using a Hybrid Monolithic Bioreactor. *ChemSusChem* **2016**, 9, 2917–2921.

(53) Chen, Z. W.; Zhou, L.; Bing, W.; Zhang, Z. J.; Li, Z. H.; Ren, J. S.; Qu, X. G. Light Controlled Reversible Inversion of Nanophosphor–Stabilized Pickering Emulsions for Biphasic Enantioselective Biocatalysis. *J. Am. Chem. Soc.* **2014**, 136, 7498–7504.

(54) Martínez, L. E.; Leighton, J. L.; Carsten, D. H.; Jacobsen, E. N. Highly Enantioselective Ring Opening of Epoxides Catalyzed by (salen)Cr(III) Complexes. *J. Am. Chem. Soc.* **1995**, 117, 5897–5898.

(55) Song, C. E.; Oh, C. R.; Roh, E. J.; Choo, D. J. Cr(salen) Catalysed Asymmetric Ring Opening Reactions of Epoxides in Room Temperature Ionic Liquids. *Chem. Commun.* **2000**, 1743–1744.

(56) Dioos, B. M. L.; Jacobs, P. A. Heterogenisation of Dimeric Cr(salen) with Supported Ionic Liquids. *J. Catal.* **2006**, 243, 217–219.

(57) Tsuji, J. *Palladium Reagents and Catalysts*. Wiley and Sons, New York, 1995.

(58) Vittoz, P. F.; Siblani, H. E.; Bruma, A.; Rigaud, B.; Sauvage, X.; Fernandez, C.; Vicente, A.; Barrier, N.; Malo, S.; Levillain, J.; Gaumont, A. C.; Dez, I. Insight in the Alginate Pd–Ionogels–Application to the Tsuji–Trost Reaction. *ACS Sustainable Chem. Eng.* **2018**, 6, 5192–5197.

TOC:

Homogeneous catalysis   Heterogeneous catalysis

Ⓐ Ⓑ ⟶ Reactants   Ⓒ ⟶ Product   Catalytic active species